Improved Performance and Stability of Organic Solar Cells by the Incorporation of a Block Copolymer Interfacial Layer

Gabriel E. Pérez,* Harikrishna Erothu, Paul D. Topham, Francesco Bastianini, Tarek I. Alanazi, Gabriel Bernardo, Andrew J. Parnell, Stephen M. King, and Alan D. F. Dunbar

In a proof-of-concept study, this work demonstrates that incorporating a specifically designed block copolymer as an interfacial layer between a charge transport layer and the photoactive layer in organic solar cells can enhance the interface between these layers leading to both performance and stability improvements of the device. This is achieved by incorporating a $P3HT_{50}$-*b*-PSS_x block copolymer as an interfacial layer between the hole transporting and photoactive layers, which results in the improvement of the interfacial roughness, energy level alignment, and stability between these layers. Specifically, the incorporation of a 10 nm $P3HT_{50}$-*b*-PSS_{16} and a 13 nm $P3HT_{50}$-*b*-PSS_{23} interfacial layer results in a 9% and a 12% increase in device efficiency respectively compared to the reference devices. In addition to having a higher initial efficiency, the devices with the block copolymer continue to have a higher normalized efficiency than the control devices after 2200 h of storage, demonstrating that the block copolymer not only improves device efficiency, but crucially, prevents degradation by stabilizing the interface between the hole transporting layer and the photoactive layer. This study proves that appropriately designed and optimized block copolymers can simultaneously stabilize and improve the efficiency of organic solar cells.

1. Introduction

Organic solar cells (OSCs) have been intensively researched during the past two decades due to their simple processability,

good mechanical flexibility, and low-cost fabrication.[1–3] Low power conversion efficiency (PCE), one of the main challenges for OSCs, has been gradually overcome by the synthesis of specifically tuned donor materials[4] such as PTB7,[5] PffBT4T-2OD,[6] PBDTTT-EFT,[7] PBDB-T-Cl,[8] and light absorbing nonfullerene acceptors[9] such as TPB,[10] ITIC,[11] IT-4F,[12] BTPTT-4F,[13] BTP-4Cl,[14] and Y6[15] achieving PCEs between 10% and 16%. Recently, a PCE of 18.22% for an OSC was reported, clearly demonstrating their promising future.[16] Despite this enticing progress, the relatively low stability of OSCs compared to other commercially available photovoltaic devices such as crystalline silicon remains the major challenge for the successful commercialization of OSC technology.[17–20] Therefore, the development of methodologies that simultaneously improve the efficiency and stability of OSCs can significantly contribute to their progress toward large-scale production. In this proof-of-concept study, a new approach to achieving this dual aim in OSCs is demonstrated. By specifically designing and incorporating an interfacial block copolymer layer whose two different blocks are selectively compatible with the photoactive layer and

Dr. G. E. Pérez, F. Bastianini, Dr. A. D. F. Dunbar
Department of Chemical and Biological Engineering
University of Sheffield
Sheffield S1 3JD, UK
E-mail: geperez1@sheffield.ac.uk

Dr. H. Erothu
Centre for Advanced Energy Studies (CAES)
Koneru Lakshmaiah Education Foundation (KLEF)
Green Fields, Vaddeswaram, Guntur, Andhra Pradesh 522 502, India

Prof. P. D. Topham
Aston Institute of Materials Research
Aston University
Birmingham B7 4AG, UK

T. I. Alanazi, Dr. A. J. Parnell
Department of Physics and Astronomy
University of Sheffield
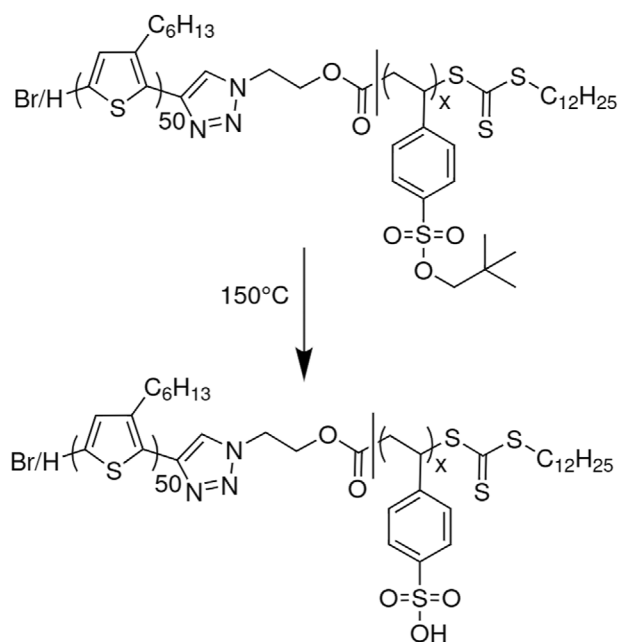Sheffield S3 7RH, UK

Dr. G. Bernardo
LEPABE - Laboratory for Process Engineering, Environment, Biotechnology and Energy
Faculty of Engineering
University of Porto
Porto 4200-465, Portugal

Dr. S. M. King
ISIS Pulsed Neutron and Muon Source
STFC
Rutherford Appleton Laboratory
Didcot OX11 0QX, UK

the hole transporting layer of the device, both the efficiency and stability of the devices are increased. Since P3HT:PCBM based OSCs are among the few OSCs materials systems that have been successfully scaled up[21–23] and are arguably the most investigated and well-known type of OSCs active layer blend,[24–29] the first device architecture that this new concept was applied to was ITO/PEDOT:PSS/P3HT:PCBM/Al. Since this architecture and these materials are well understood, the effects of the interfacial block copolymer can be more easily singled out, corroborated, and understood. In the remainder of this section, the P3HT:PCBM and PEDOT:PSS interface as well as the design of the block copolymer are discussed.

Poly(3,4-ethylenedioxythiophene):poly(styrene sulfonate) (PEDOT:PSS) is one of the most commonly used hole transporting layers (HTL) in OSCs, particularly in P3HT based OSCs, due to its simple processability, high transparency to most of the solar spectrum when processed as a thin film,[30] good mechanical and thermal stability,[31–33] and excellent water solubility.[34] However, the PEDOT:PSS/P3HT:acceptor interface is far from optimal as it exhibits poor adhesion and an unfavorable surface energy difference between adjacent layers.[35–37] Moreover, it has been shown before that PEDOT:PSS coated films have a surface rich in PSS with the sulphate group oriented toward the surface.[38,39] This allows a reaction to occur between PSS and P3HT that results in the p-doping of P3HT and its degradation due to the highly acidic nature of PSS.[40] Additionally, if a ≥150 °C thermal annealing treatment is applied during device fabrication after the P3HT based layer has been deposited on the PEDOT:PSS for improved performance, the PSS intermixes with P3HT[39] which reduces the efficiency of the device. Several efforts to improve the interface between PEDOT:PSS and P3HT have been made mainly by doping PEDOT:PSS with different substances in order to change its physical and chemical properties such as selective carrier blocking and mobility, PSS content, and morphology resulting in the improved performance and stability of the device.[41–44] However, since the morphological changes that PEDOT:PSS experiences after being doped are complex,[45] and to an extent not completely understood, this route toward improving the compatibility between PEDOT:PSS and P3HT:acceptor can be unreliable. Therefore, a different approach to improving the compatibility between PEDOT:PSS and P3HT:PCBM is adopted here.
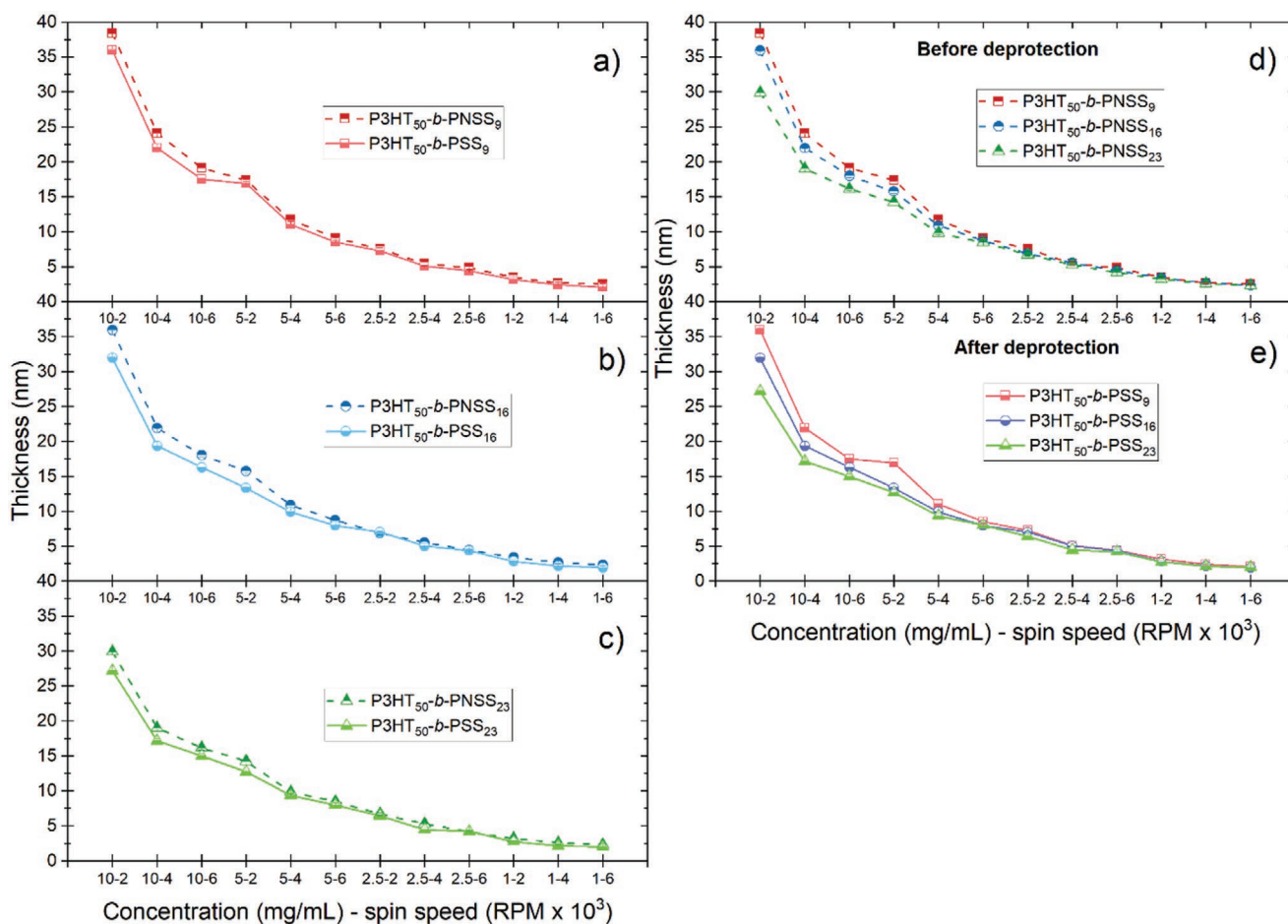
Block copolymers have been extensively used as compatibilizers,[46–48] templating agents,[49,50] active materials,[51–53] and electrode-active layer interfacial materials,[54,55] to improve the efficiency and stability of organic solar cells. This is due to the advantageous thermodynamic incompatibility between the different blocks in the block copolymer.[56,57] This incompatibility allows the block copolymer to separate into different domains of the polymer constituents on the nanoscale, while remaining linked on the macroscale due to the covalent binding of the blocks. These features have enabled the possibility to control of the microphase separation of donor–acceptor blends and the possibility to prevent the macro-phase degradation, features that are paramount to improve the efficiency and stability of devices.[58–60] Moreover, each block in the block copolymer can have different interactions with the different components of the surrounding environment of the block copolymer depending

Figure 1. Chemical structure of P3HT-*b*-PNSS (top). The neopentyl group is removed with a 150 °C thermal annealing treatment to produce P3HT-*b*-PNSS (bottom).

on the composition and properties of the blocks. In a previous study, we reported the synthesis and characterization of a poly(3-hexylthiophene)-*b*-poly(neopentyl p-styrenesulfonate) (P3HT-*b*-PNSS) block copolymer that upon deposition, is thermally treated at 150 °C to be converted into P3HT-*b*-PSS (**Figure 1**). The motivation to synthesize this block copolymer was to use it as an interfacial layer between the PEDOT:PSS hole transporting layer (HTL) and the P3HT:PCBM photoactive active layer (PAL) in OSCs to prevent degradation mechanisms between the HTL and the PAL. The design of this block copolymer was intended to allow the P3HT block to interact and enhance adhesion with the P3HT based PAL, and the PSS block to engage in electrostatic interactions with the PEDOT:PSS HTL. Due to the polar nature of PSS, the neopentyl group was added to the preannealed block copolymer to enable its solubility in a common organic solvent.[61] However, it was necessary to remove the neopentyl group once the block copolymer has been deposited to avoid its subsequent dissolution due to the coating of the next layer, which is often dissolved in an organic solvent that could otherwise dissolve the block copolymer. The removal of the neopentyl group of the deposited film, thus, can be achieved by a 150 °C thermal annealing treatment, which renders the block copolymer insoluble in organic solvents. In the synthesis report, the block copolymers were incorporated into P3HT based devices as part of a preliminary study, however, since the focus of that study was reporting the synthesis of the block copolymers, their optimization as functional interfacial layers in the devices was not done. This resulted in the poor performance of the devices with the block copolymer incorporated within their architecture compared to the control devices without any block copolymer.

In this study, three variants of P3HT-*b*-PNSS with different PSS block lengths were incorporated as interfacial layers with

ADVANCED
Science News

www.advancedsciencenews.com

ADVANCED
MATERIALS
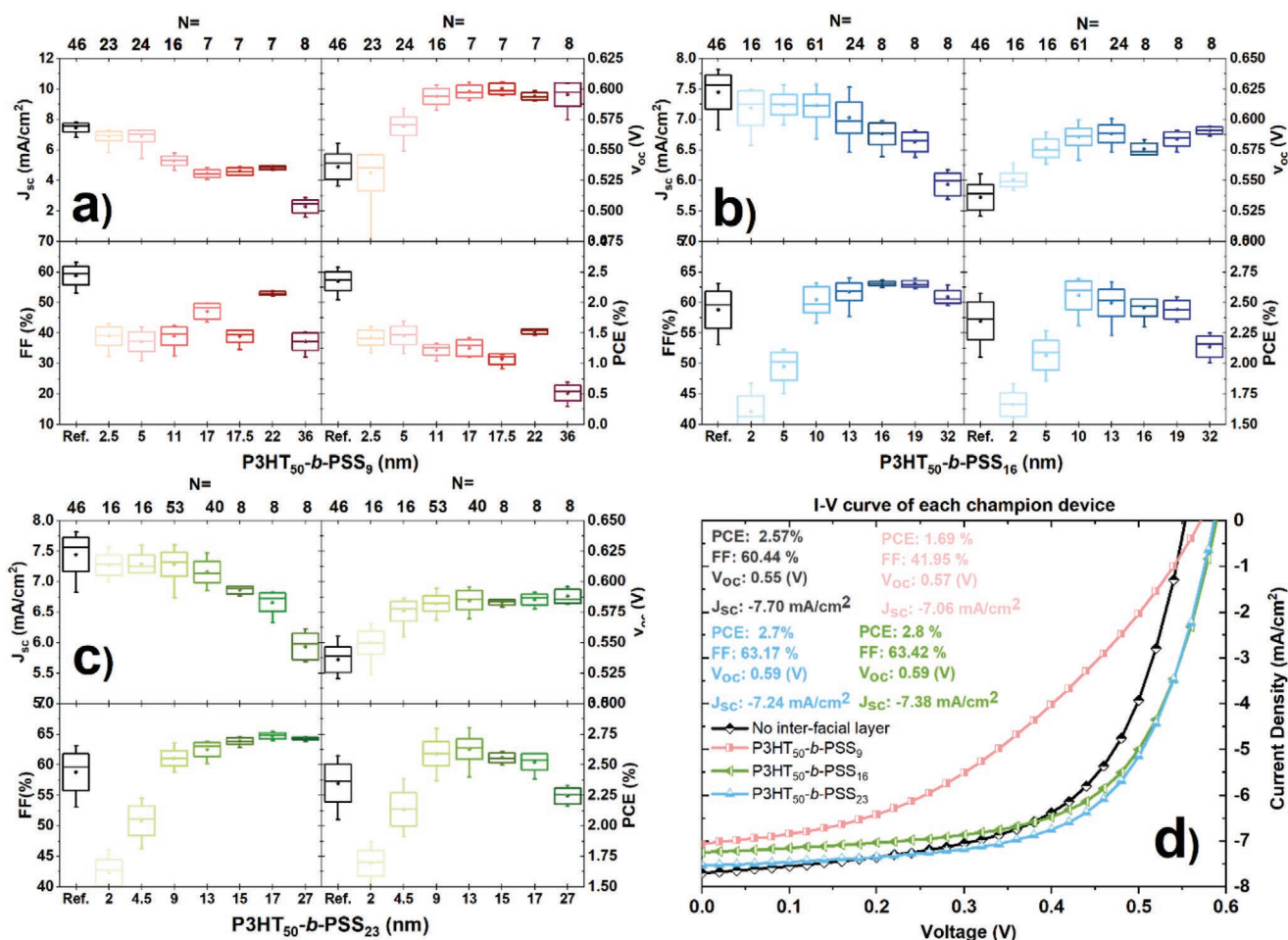**INTERFACES**

www.advmatinterfaces.de

Figure 2. Thickness of the block copolymers films as a function of concentration and spin speed as measured by ellipsometry. The first digit of the x-axis labels indicates the concentration of the solution in mg mL^{-1}, and the second digit indicates the spin speed in thousands of RPM. Error bars for each data point are included in this figure representing the one standard deviation on each side of the average value given by the CompleteEASE software, however due to the accuracy of the technique the error bars are significantly small. Figures a, b, and c show the thickness of each block copolymer respectively, before and after deprotection, while figures d and e show a comparison of the three block copolymers before and after deprotection, respectively.

varying thicknesses between PEDOT:PSS and P3HT:PCBM in normal architecture OSCs. The most successful block copolymer variant improved the compatibility between adjacent layers, which is reflected by a 9% increase in open circuit voltage (V_{oc}) and a 6.2% increase in fill factor (FF) which result in a 12% relative increase in power conversion efficiency (PCE) despite a 4.0% decrease in short-circuit current (J_{sc}). The enhanced V_{oc} owes its improvement to a more beneficial energy level transition for holes provided by the block copolymer. The improved FF is allowed by the enhanced contact between the HTL and P3HT that the block copolymer provides due to its smoother surface compared to PEDOT:PSS, and the compatibility of each block in the block copolymer with the adjacent layers. Finally, it is demonstrated that the block copolymer stabilizes the interface and acts as a barrier preventing long term degradation originating from the reaction between the HTL and PAL. Our study demonstrates that specifically designed block copolymers can be incorporated as interfacial layers between the HTL and PAL of OSCs to enhance the photovoltaic performance and stability of the devices. This approach also holds promise for interface management in other types of solar cells such as perovskite solar cells.

2. Results and Discussion

2.1. Thickness of Block Copolymers Films

An important issue to consider when using an interfacial layer based on P3HT in the transparent part of the conventional device structure (e.g., between the HTL and the PAL) is the absorption of light by the P3HT component in such an interfacial layer. This results in less light reaching the active layer, where efficient charge separation can occur, and hence less current generated by the device. One way to address this issue is by controlling the thickness of the film. The thinnest interfacial film allows for maximum transparency. However, if the film is too thin the quality of the contact between the PEDOT:PSS and the P3HT:PCBM films is hindered, which decreases the fill factor of the devices. First, different thicknesses of the block copolymers films resulting from different processing conditions were determined. Four different solution concentrations of each block copolymer (1, 2.5, 5, and 10 mg mL^{-1}) were prepared and spin-cast at three different speeds (2000, 4000, and 6000 RPM) to obtain 12 different thicknesses

ADVANCED
SCIENCE NEWS
www.advancedsciencenews.com

ADVANCED
MATERIALS
INTERFACES
www.advmatinterfaces.de

Figure 3. Box plots showing the photovoltaic performance (short circuit current, open circuit voltage, fill factor, and power conversion efficiency) of the OSC devices with a) P3HT$_{50}$-*b*-PSS$_9$, b) P3HT$_{50}$-*b*-PSS$_{16}$, and c) P3HT$_{50}$-*b*-PSS$_{23}$ incorporated in varying thicknesses as interfacial layers between the PEDOT:PSS and P3HT:PCBM layers. N equals the number of different measurements for each type of device, the height of the box represents one standard deviation from the mean average value, the top and bottom ticks are the maximum and minimum values respectively, the horizontal line within the box is the median, and the circle in the middle of the box is the mean average value. The *J–V* curve d) of each champion device is also shown for performance comparison.

for each block copolymer as measured with ellipsometry. As shown in **Figure 2**d and Table S3 in the Supporting Information, the thickness of the three types of block copolymer films decreases as the concentration of the solution decreases and as the spin speed increases. This trend is expected; however, the results also show that the thickness of the block copolymer films have an additional dependence on the length of the PNSS chain. The longest PNSS chains result in the thinnest films under the same processing conditions. This effect is more significant at higher thicknesses. To investigate the origin of the block copolymer film thickness dependence on the length of the PNSS chain, small angle neutron scattering (SANS) was used to study the block copolymer solutions and to determine their radius of gyration (see Figure S1 and Table S1 in the Supporting Information). It was concluded that the lower solubility of PNSS causes it to be more densely packed in the solution than P3HT. This results in the decreased radius of gyration of the block copolymers with the longer PNSS lengths. Therefore, the block copolymers with the longer PNSS lengths become more tightly packed

in solution which subsequently results in a lower volume film when spin-cast (see discussion in S-2–S-4, Supporting Information). As previously mentioned, in order for the block copolymer films to function as originally intended in OSCs, the polar properties of the PNSS block must be restored by removing the neopentyl group. This is achieved by a thermal deprotection process in which the block copolymer films are annealed at 150 °C for 3 h. Thermal annealing is also known to affect the thickness of P3HT-based polymers[62] due to the reordering of its polymer chains and increased crystallinity,[63,64] and since the block copolymers are composed mostly of P3HT, it is expected that they will experience a similar effect. In order to obtain the actual thickness values of the block copolymer films that will be incorporated in the devices, their thickness after the deprotection process was also measured by ellipsometry and found to be slightly reduced by the thermal deprotection process. Interestingly, the reduced thickness caused by the thermal annealing deprotection step was more significant for thicker films (see Figure 2a–c). In addition to the increased crystallinity mentioned above, the

Table 1. Photovoltaic performance metrics of OSC devices with the different block copolymers incorporated as interfacial layers with varying thicknesses between PEDOT:PSS and P3HT:PCBM. The error values represent the standard deviation for "N" number of different measurements.

	Average				Champion device				N
	J_{sc} [mA cm^{-1}]	V_{oc} [V]	FF [%]	PCE [%]	J_{sc} [mA cm^{-1}]	V_{oc} [V]	FF [%]	PCE [%]	
Reference	**7.45 ± 0.28**	**0.536 ± 0.010**	**58.82 ± 3.00**	**2.35 ± 0.16**	**7.82**	**0.555**	**63.14**	**2.57**	**46**
P3HT$_{50}$-b-PSS$_9$ [nm]									
2.5	6.89 ± 0.30	0.531 ± 0.015	38.95 ± 3.01	1.42 ± 0.12	7.27	0.546	43.05	1.61	23
5	6.90 ± 0.38	0.569 ± 0.008	37.16 ± 3.15	1.46 ± 0.15	7.24	0.584	41.95	1.69	24
11	5.58 ± 0.31	0.594 ± 0.006	37.16 ± 3.18	1.46 ± 0.15	7.24	0.584	41.95	1.33	7
17	4.44 ± 0.26	0.598 ± 0.005	47.07 ± 2.54	1.25 ± 0.14	4.84	0.605	49.83	1.43	7
17.5	4.59 ± 0.23	0.600 ± 0.004	38.90 ± 2.02	1.07 ± 0.08	4.88	0.606	40.98	1.15	7
22	4.84 ± 0.12	0.594 ± 0.003	53.02 ± 0.55	1.52 ± 0.04	4.99	0.599	53.8	1.56	7
36	2.29 ± 0.42	0.595 ± 0.010	37.12 ± 2.83	0.51 ± 0.13	2.86	0.605	40.22	0.7	8
P3HT$_{50}$-b-PSS$_{16}$ [nm]									
2	7.18 ± 0.28	0.550 ± 0.006	42.09 ± 2.59	1.66 ± 0.09	7.5	0.564	46.73	1.83	16
5	7.24 ± 0.16	0.576 ± 0.001	49.51 ± 2.28	2.07 ± 0.12	7.56	0.59	52.32	2.26	16
10	**7.22 ± 0.19**	**0.586 ± 0.007**	**60.46 ± 2.14**	**2.56 ± 0.12**	**7.57**	**0.6**	**63.17**	**2.7**	**61**
13	7.03 ± 0.26	0.588 ± 0.007	61.74 ± 1.44	2.50 ± 0.11	7.53	0.601	64.06	2.67	24
16	6.76 ± 0.18	0.576 ± 0.005	63.10 ± 0.38	2.46 ± 0.07	6.98	0.58	63.65	2.52	8
19	6.63 ± 0.16	0.584 ± 0.006	63.06 ± 0.55	2.44 ± 0.08	6.81	0.591	63.94	2.54	8
32	5.93 ± 0.17	0.591 ± 0.003	60.91 ± 0.01	2.14 ± 0.09	6.18	0.594	62.83	2.25	8
P3HT$_{50}$-b-PSS$_{23}$ [nm]									
2	7.2 ± 0.16	0.50 ± 0.009	42.2 ± 2.15	1.6 ± 0.11	7.56	0.566	46.08	1.87	16
5	7.2 ± 0.14	0.56 ± 0.008	50.8 ± 2.42	2.1 ± 0.14	7.6	0.586	54.53	2.4	16
9	7.2 ± 0.20	0.52 ± 0.006	61.0 ± 1.26	2.5 ± 0.10	7.6	0.595	63.56	2.8	53
13	**7.1 ± 0.17**	**0.55 ± 0.008**	**62.4 ± 1.14**	**2.6 ± 0.08**	**7.47**	**0.596**	**63.85**	**2.8**	**40**
15	6.8 ± 0.06	0.53 ± 0.002	63.8 ± 0.53	2.5 ± 0.04	6.93	0.585	64.54	2.61	8
17	6.6 ± 0.15	0.55 ± 0.005	64.7 ± 0.50	2.5 ± 0.07	6.82	0.591	65.44	2.6	8
27	5.9 ± 0.22	0.58 ± 0.006	64.3 ± 0.22	2.2 ± 0.06	6.22	0.596	64.54	2.33	8

decreased thickness is also likely to be caused by the evaporation of any residual chlorobenzene solvent in the films, which has a boiling point of 132 °C. Moreover, the removal of the neopentyl protecting group by the thermal annealing step also contributes to the reduced thickness of the film. The effects of the thermal deprotection process on the block copolymers were further investigated with UV-vis spectroscopy and atomic force microscopy, and discussed in pages S-5 to S-8 (Supporting Information).

2.2. Photovoltaic Performance of Devices

The block copolymers were incorporated (into OSCs) as interfacial films in seven different thicknesses and the photovoltaic performance of the devices was measured. Devices with the structure ITO/PEDOT:PSS/P3HT-b-PSS/P3HT:PCBM/Al were fabricated in air (except for the deprotection process) and without an electron transport layer for simplicity and industry scalable feasibility (the individual processing steps are shown in Figure S10 in the Supporting Information). The photovoltaic performance of the devices is shown in **Figure 3** and **Table 1**. The average PCE, FF, V_{oc} and J_{sc} of the reference devices were 2.35±0.16%, 58.82±3.00%, 0.536±0.010 V, and 7.45±0.28 mA cm^{-2}, respectively, which are comparable to the values obtained in literature for this type of device structure.[65–68] The incorporation of the block copolymer with the shortest PSS block, P3HT$_{50}$-b-PSS$_9$, resulted in a decreased performance irrespective of the thickness. However, the incorporation of the block copolymers with the longer PSS blocks, P3HT$_{50}$-b-PSS$_{16}$ and P3HT$_{50}$-b-PSS$_{23}$, resulted in the optimally improved efficiency of the devices relative to the reference devices by 9%, and 12%, when processed as 10 and 13 nm films, respectively. The devices with a 10 nm thick P3HT$_{50}$-b-PSS$_{16}$ interfacial layer had a PCE of 2.56±0.12%, while the PCE of the devices with a 13 nm thick P3HT$_{50}$-b-PSS$_{23}$ interfacial layer had a PCE of 2.63±0.08%. The enhanced efficiency in both type of devices is mainly caused by a 9% increase in the V_{oc} which was 0.586±0.007 V for the P3HT$_{50}$-b-PSS$_{16}$ incorporated device and 0.585±0.008 V for P3HT$_{50}$-b-PSS$_{23}$ incorporated device. It is worth noting that even though devices incorporating a P3HT$_{50}$-b-PSS$_9$ had a significantly lower photovoltaic performance than the reference device, their V_{oc} increased by approximately the same amount as the increase in V_{oc} of the P3HT$_{50}$-b-PSS$_{16}$ and P3HT$_{50}$-b-PSS$_{23}$ incorporated devices.

This is an indication of an improved energy level alignment at the interface caused by the block copolymer. A slight increase of 2.8% and 6.2% in fill factor of the devices with the 10 nm P3HT$_{50}$-b-PSS$_{16}$ (60.46±2.14%) and the 13 nm P3HT$_{50}$-b-PSS$_{23}$ (62.49±1.14%) films, respectively, also contributed to the improved PCE. The increased V_{oc} and FF of the devices with the 10 and 13 nm block copolymer incorporated films more than compensate for the expected decrease in J_{sc} by 3.2% and 4.0%, respectively, caused by the light absorbance of the block copolymer layer. The J_{sc} of the devices with P3HT$_{50}$-b-PSS$_{16}$ incorporated was 7.22 ± 0.19 mA cm^{-2} while the J_{sc} of the devices with P3HT$_{50}$-b-PSS$_{23}$ incorporated had a J$_{sc}$ of 7.16 ± 0.17 mA cm^{-2}.
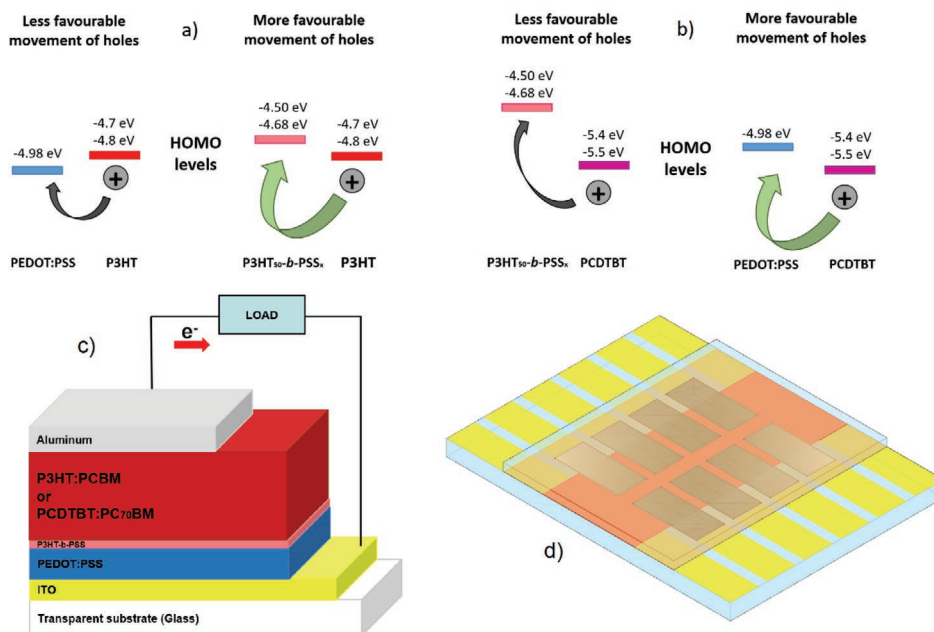
2.3. Energy Band Alignment of the Block Copolymers

To determine the origin of the improved V_{oc}, the energy levels of the PEDOT:PSS and the block copolymers were studied. It is well known that the V_{oc} of OSCs has a strong dependence on the alignment of the energy levels of the different materials within its structure.[69–71] The HOMO level of a P3HT thin film ($\approx$100 nm) with a weight average molecular weight (M_w) of more than 30 000 measured with ultraviolet photoelectron spectroscopy (UPS) has been reported to be in the range of -4.8 to -4.7 eV.[72,73] For holes to efficiently move into the HTL, thus avoiding significant V_{oc} losses, the HTL must have a HOMO higher than that of P3HT. To determine if this is the case for the structure of the reference device, the HOMO of a PEDOT:PSS film equal to the one used in the devices was determined with UPS. It was found that the HOMO level of the PEDOT:PSS film was -4.98 eV (agreeing with the value provided by the manufacturer) which is lower than the HOMO level of P3HT. This is nonideal for holes transport since it presents a barrier of $\approx$0.2 eV, hindering their transport to the PEDOT:PSS from the P3HT. This results in V_{oc} losses due to the recombination events caused by the holes that are not able to move to the PEDOT:PSS HTL,[69] and the excitons that are not successfully dissociated at the PEDOT:PSS-P3HT:PCBM interface. The HOMO levels of 11 nm P3HT$_{50}$-b-PSS$_9$, 10 nm P3HT$_{50}$-b-PSS$_{16}$, and 13 nm P3HT$_{50}$-b-PSS$_{23}$ thin films were determined to be -4.50, -4.55, and -4.68 eV respectively. The UPS measurements on the block copolymers confirmed that they have a higher HOMO than the P3HT, which facilitates the transfer of holes from the P3HT to the block copolymers compared to the transfer of holes from P3HT to PEDOT:PSS. Therefore, the HOMO levels of the block copolymers provide a more favorable energy level than PEDOT:PSS for the holes generated in P3HT to travel into. This also implies that it is highly likely that the excitons generated close enough to travel to the interface between the block copolymers and the active layer can dissociate more favorably than the excitons at the interface between PEDOT:PSS and P3HT in the reference device. The more energetically favorable level provided by the block copolymers results in lower voltage losses and thus, a higher V_{oc} of the devices with the incorporated block copolymers. This is further confirmed by the fact that the improved V_{oc} of the devices with the block copolymers was increased by approximately the same amount relative to the reference device (see Figure 3 and Table 1) irrespective of the processing conditions of the block copolymer (i.e., resulting thickness, and hence UV–vis transmittance). It is worth mentioning that the holes in the block copolymer layer would still have to overcome an unfavorable energy alignment to travel into the PEDOT:PSS. However, it is proposed that the electrostatic interactions between the PEDOT:PSS layer and the PSS block in the block copolymer result in the formation of an intermixed interface which results in band-bending of the HOMO of the PEDOT:PSS to a higher energy level more similar to the one of the block copolymer. This enables the good transition of holes from the block copolymer into the PEDOT:PSS. It is also possible that the block copolymer film prevents the contact between the PCBM and the PEDOT:PSS ensuring that electrons do not leak into the PEDOT:PSS and eventually to the ITO electrode. The block copolymer can then be conceptualized as an additional filter that prevents electrons from reaching the hole conducting electrode, and thus avoiding more recombination events that decrease V_{oc} of the device. The photoelectron spectra of each film is shown in the supporting information (Figures S6–S9, Supporting Information).

To confirm that the improved V_{oc} for the devices incorporating the block copolymer is due to the beneficial HOMO levels provided by the block copolymers for the holes to move from the P3HT, the 4.5, 9, 13, and 17 nm P3HT$_{50}$-b-PSS$_{23}$ films were also incorporated into PCDTBT devices. Since PCDTBT has a HOMO level (-5.4 to -5.5[44]) lower than both PEDOT:PSS and the block copolymer, the holes in PCDTBT would relax more favorably to PEDOT:PSS than to the block copolymer. This is due to the fact that the HOMO level of PEDOT:PSS (-4.98 eV) is closer to the HOMO of PCDTBT than the HOMO of P3HT$_{50}$-b-PSS$_{23}$ (-4.68 eV). Therefore, it was expected that incorporating P3HT$_{50}$-b-PSS$_{23}$ into PCDTBT devices would detrimentally affect the V_{oc} of the devices. Moreover, since the PCDTBT donor is not as compatible with the P3HT block in the block copolymers, it is also expected that the fill factor and the overall photovoltaic performance of the device will be lower than the PCDTBT reference devices without the interfacial P3HT$_{50}$-b-PSS$_{23}$ layer. The photovoltaic performance of the PCDTBT based devices are shown in Figure S11 and Table S4 (Supporting Information).

As predicted, the average V_{oc} of the PCDTBT devices with a P3HT$_{50}$-b-PSS$_{23}$ interfacial layer was lower (0.644 ± 0.018, 0.638 ± 0.011, 0.615 ± 0.004, and 0.666 ± 0.011 V for the 4.5, 9, 13, and 17 nm thick films, respectively) than the average V_{oc} of the reference device (0.850 ± 0.021 V) regardless of the thickness of the block copolymer used. It is highly likely that the reason behind the reduced V_{oc} in the PCDTBT devices incorporating P3HT$_{50}$-b-PSS$_{23}$ compared to the reference devices is the increased voltage losses caused by the higher difference in energy between the HOMO of PCDTBT and the HOMO of P3HT$_{50}$-b-PSS$_{23}$ compared to that between the HOMO of PCDTBT and the HOMO of PEDOT:PSS (see **Figure 4**). The FF of the PCDTBT devices incorporating P3HT$_{50}$-b-PSS$_{23}$ (39.82 ± 0.87, 43.19 ± 0.87, 44.12 ± 0.91, and 44.98 ± 2.48% for the 4.5, 9, 13, and 17 nm thick films, respectively) was also lower than the FF of the reference device (53.56 ± 3.98%) regardless of the thickness of the block copolymer. This could indicate that indeed the contact between the P3HT$_{50}$-b-PSS$_{23}$ interfacial layer and PCDTBT is poor, resulting in an increased series resistance within the devices.
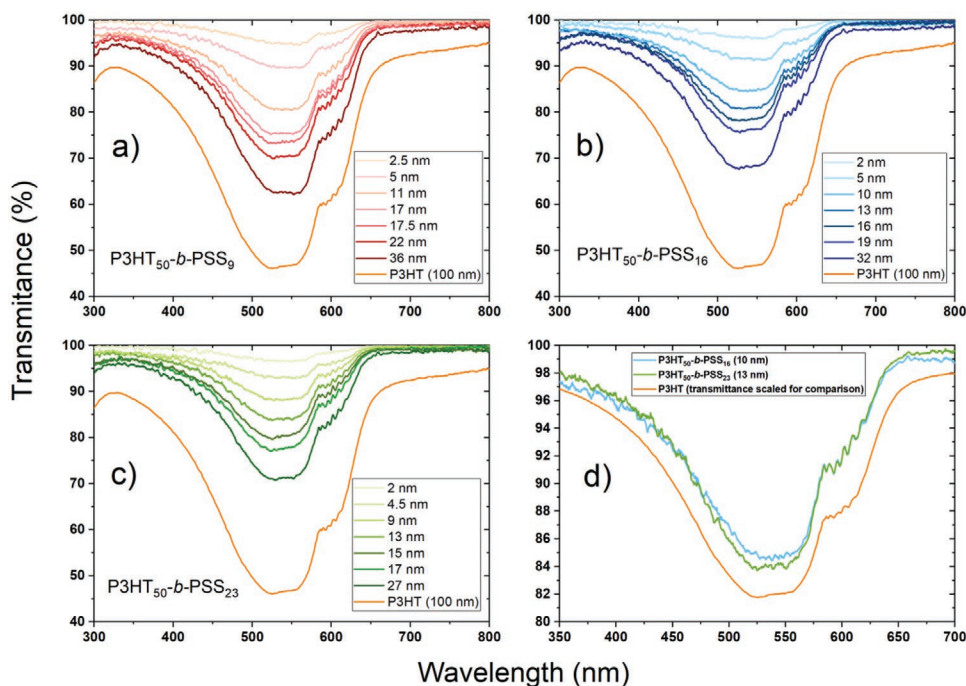
Figure 4. Hole transition from a) P3HT and b) PCDTBT to either PEDOT:PSS or P3HT$_{50}$-b-PSSx. c) A cross sectional view of the device structure, and d) a top view of the devices are shown for comparison.
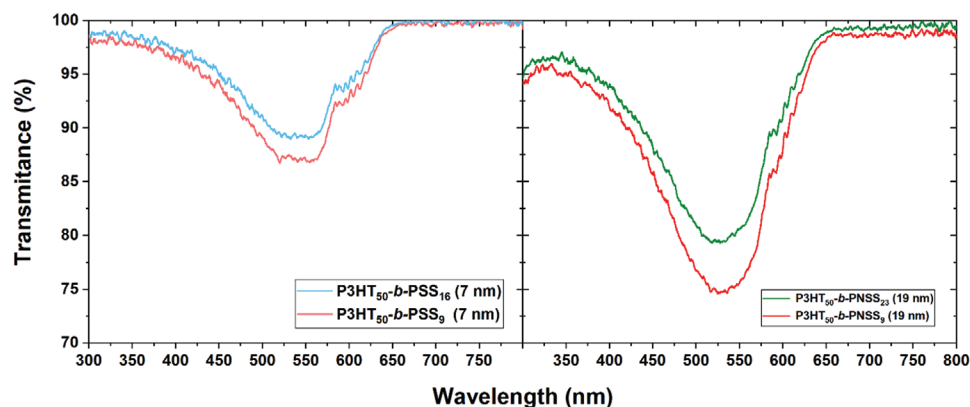
2.4. Transparency of Block Copolymers

In order to corroborate that the decrease in J_{sc} of the P3HT devices incorporating the block copolymers is caused mainly by the light absorption of the block copolymers, the UV–vis transmittance of the seven films (after deprotection) of different thicknesses of each block copolymer used for device fabrication was measured. **Figure 5**a–c shows the transmission spectra of the block copolymers where the three characteristic vibronic shoulders of P3HT films at $\lambda = 520$ nm, $\lambda = 554$ nm, and at

Figure 5. UV–vis transmittance of a) P3HT$_{50}$-b-PSS$_9$, b) P3HT$_{50}$-b-PSS$_{16}$, and c) P3HT$_{50}$-b-PSS$_{23}$ deposited as seven different thickness films. d) The spectra of the 10 nm P3HT$_{50}$-b-PSS$_{16}$ and 13 nm P3HT$_{50}$-b-PSS$_{23}$ films which resulted in the best performing devices when incorporated into the OSC are shown separately for comparison.

**ADVANCED
SCIENCE NEWS**

www.advancedsciencenews.com

**ADVANCED
MATERIALS
INTERFACES**

www.advmatinterfaces.de

Figure 6. (Left) UV–vis transmittance of the deprotected 7 nm $P3HT_{50}$-b-PSS_9 and $P3HT_{50}$-b-PSS_{16} films. (Right) UV–vis transmittance of the non-deprotected 19 nm $P3HT_{50}$-b-$PNSS_9$ and the $P3HT_{50}$-b-PSS_{23} films.

$\lambda = 610$ nm can be immediately identified.[74,75] This is expected since the block copolymer contains P3HT. It is worth noting that PSS absorbs in the ultraviolet region ($\lambda < 300$ nm) of the electromagnetic spectrum[76] and therefore, does not show in these spectra. Moreover, the transmittance of the three block copolymer films decreases as their thicknesses increase which indicates an increased absorption of light by the thicker films. This is consistent with the decrease in J_{sc} of the devices shown in Figure 3 which is also correlated to the increase in thickness of the block copolymers films. This is further confirmed by Figure 5d which shows that the transmittance minima of the 13 nm $P3HT_{50}$-b-PSS_{23} film is slightly lower (83.9% at $\lambda = 520$ nm) than that of the 10 nm $P3HT_{50}$-b-PSS_{23} film (85.0% at $\lambda = 520$ nm) which explains the reduced J_{sc} of the devices incorporating the $P3HT_{50}$-b-PSS_{23} block copolymer compared to the ones with $P3HT_{50}$-b-PSS_{16}.
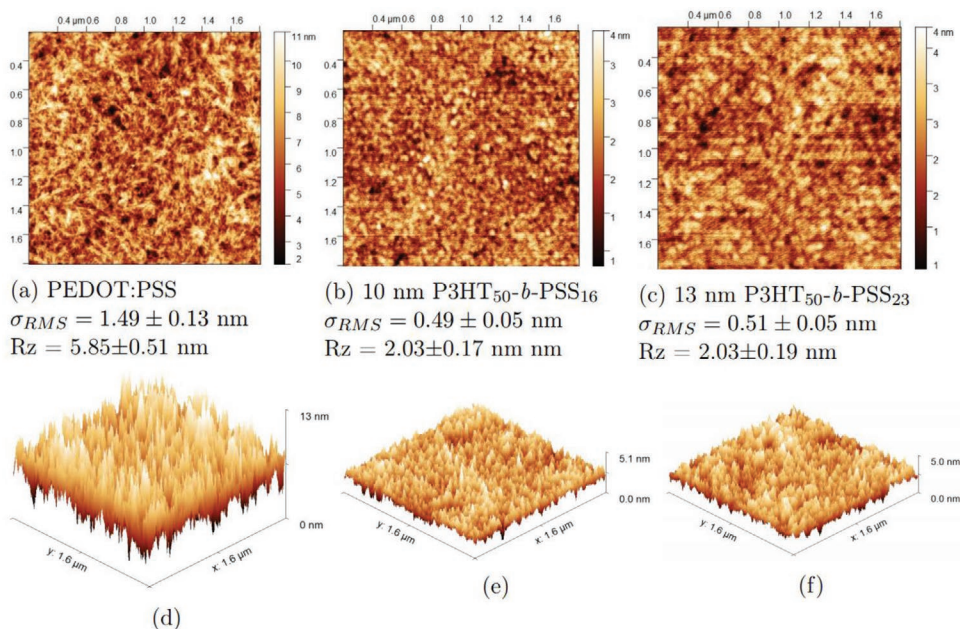
The UV–vis data also show that the block copolymer films with the longer PSS blocks have lower transmittance than the block copolymer films with the shorter PSS blocks even if the different films have the same thickness. **Figure 6** compares the UV–vis spectra of the 7 nm $P3HT_{50}$-b-PSS_9 and the 7 nm $P3HT_{50}$-b-PSS_{16} deprotected films. Despite having the same thickness, the $P3HT_{50}$-b-PSS_{16} film has a higher transmittance than the $P3HT_{50}$-b-PSS_9 film. Since both films were cast from solutions with the same concentration of block copolymer (2.5 mg mL^{-1}) and the solutions were prepared by weight, this can be explained by the $P3HT_{50}$-b-PSS_{16} film having a lower relative amount of P3HT compared to the $P3HT_{50}$-b-PSS_9 film. This trend is also shown by the non-deprotected films as seen in Figure 6; the 19 nm $P3HT_{50}$-b-PSS_{23} film has a higher transmittance than the 19 nm $P3HT_{50}$-b-PSS_9 film.

2.5. Block Copolymers Surface Topography Analysis

It is well known that the surface roughness of the different layers that comprise the structure of the device has an impact on its performance.[77–79] Specifically, some studies have attributed the improved performance of the devices to the increased fill factor.[80,81] Therefore, to investigate if the slightly increased fill factor of the devices with the 10 nm $P3HT_{50}$-b-PSS_{16} and the

13 nm $P3HT_{50}$-b-PSS_{23} films incorporated within them had a correlation with the different roughnesses of the block copolymers and the PEDOT:PSS films, their surface was analyzed by atomic force microscopy (AFM). **Figure 7**a,d shows the 2D and 3D height images, respectively, of PEDOT:PSS which has an average root mean square roughness (RMS) of 1.49 ± 0.13 nm, a value that is consistent with literature.[45,82] Meanwhile, the 10 nm $P3HT_{50}$-b-PSS_{16} (Figure 7b,e) and 13 nm $P3HT_{50}$-b-PSS_{23} (Figure 7c,f) films have a very similar RMS of 0.49 ± 0.05 and 0.51 ± 0.05 nm, respectively, which is three times lower than that of PEDOT:PSS. The smoother surface of the block copolymers will allow the formation of an enhanced contact with the P3HT:PCBM layer improving the fill factor of the device. This provides a possible explanation to why thinner block copolymer layers (<9 nm) result in a decreased fill factor when incorporated in devices (see Figure 3 and Table 1). While the 10 nm and 13 nm block copolymer films are thick enough to overcome the peak to valley average height of the PEDOT:PSS surface ($R_z = 5.85 ± 0.51$ nm), thinner films such as the 2.5 nm and 5 nm, and 2.5nm and 4.5nm of $P3HT_{50}$-b-PSS_{16} and $P3HT_{50}$-b-PSS_{23}, respectively, are sufficiently thin to have their surface roughness significantly affected by the underlying PEDOT:PSS roughness. Additionally, the <5 nm thin block copolymer films exhibit numerous aggregation points where the block copolymer forms clusters rather than forming an evenly coated surface (see S-6–S-8 in the Supporting Information). These pinholes hinder the flow of current within the device decreasing its shunt resistance and increasing its series resistance, which is evidenced by the decreased fill factor. In addition to the effect of the roughness of the block copolymers on the performance of the device, a correlation between the thickness and the FF was also found. Figure 3b,c shows that the fill factor of the devices with the $P3HT_{50}$-b-PSS_{16} and the $P3HT_{50}$-b-PSS_{23} incorporated films improves as the thickness of such block copolymers is increased. Therefore, there is a positive correlation between the thickness of the block copolymers and the FF of the device. However, if the thickness of the block copolymers is significantly high, such as the 32 nm $P3HT_{50}$-b-PSS_{16} and the 27 nm $P3HT_{50}$-b-PSS_{23} films, the overall FF of the device decreases due to the significantly decreased J_{sc} caused by the increased absorbance of light by the thick block copolymer layer. Hence, there
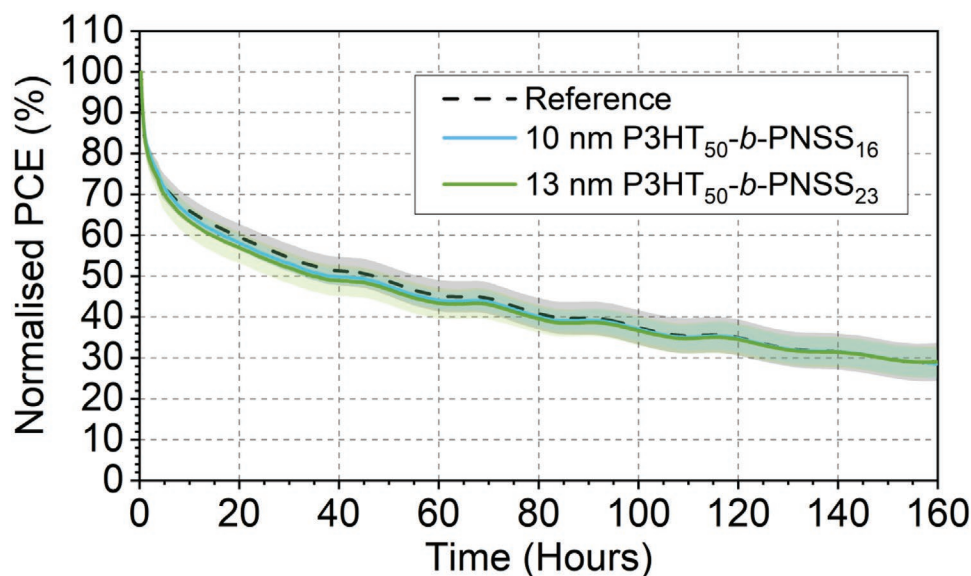
ADVANCED
SCIENCE NEWS
www.advancedsciencenews.com

ADVANCED
MATERIALS
INTERFACES
www.advmatinterfaces.de

Figure 7. AFM height 2D (top) and 3D (bottom) images of pristine PEDOT:PSS (a,d), 10 nm thick $P3HT_{50}$-b-PSS_{16} (b,e), and 13 nm thick $P3HT_{50}$-b-PSS_{23} (c,f). Root mean square roughness (RMS) and average peak to valley roughness (R_z) are shown for comparison. The errors represent one standard deviation.

is a tradeoff between maintaining a high J_{sc} and improving the FF resulting in an optimal thicknesses for device performance of 10 and 13 nm for the $P3HT_{50}$-b-PSS_{16} and the $P3HT_{50}$-b-PSS_{23} layers, respectively. It is worth noting that the smoother surface of the block copolymers is not the only contributing factor to the enhanced contact. Since the deprotected block copolymer surface is composed mostly of P3HT (see S-7–S-8 in the Supporting Information), it is likely that the P3HT chains in the active layer have an enhanced wettability with the P3HT chains in the block copolymers than with the PEDOT:PSS chains of the HTL due to their differing surface energies. Moreover, since the deprotection process promotes the segregation of PSS toward the bottom of the film[83] (see Figure S4, Supporting Information), the PSS chains in the block copolymer can take part in electrostatic interactions with the PEDOT:PSS resulting in the enhanced interfacial contact between PEDOT:PSS and the block copolymers compared to that between PEDOT:PSS and P3HT:PCBM. This also provides an explanation for the reduced photovoltaic performance of the $P3HT_{50}$-b-PSS_9 incorporated devices regardless of the block copolymer thickness used. Their low performance is attributed to insufficient PSS in the block copolymer film to provide favorable adhesion to PEDOT:PSS. Since the P3HT block is dominant in the block copolymer, the film behaves functionally as an additional P3HT layer rather than a block copolymer hindering the interfacial quality, and thus, the fill factor of the device as shown by Figure 3a.

2.6. Lifetime of Devices

Over time, the physical and chemical interactions between PEDOT:PSS and P3HT:acceptor can degrade the materials and result in detrimental effects for device performance. This interface can experience degradation mechanisms specific to the contact between the adjacent layers such as delamination, intermixing, and chemical reactivity,[35,39,40] resulting in the breakdown of device performance over time. The interfacial block copolymer incorporated between the HTL and the PAL is expected to serve as a barrier to prevent some of these processes given that, as discussed before, the P3HT block in the block copolymer comes into contact mainly with the P3HT in the PAL, and that the PSS block comes into contact with the PEDOT:PSS. Therefore, lifetime tests were conducted on the devices with the 10 nm $P3HT_{50}$-b-PSS_{16} and the 13 nm $P3HT_{50}$-b-PSS_{23} films to determine if they would degrade at a slower rate than a reference device without any block copolymer. First, a lifetime test under constant illumination was conducted. As shown in **Figure 8**, it was found that all the devices degrade at very similar rates having their PCE decreased to <30% of their initial value after 160 h. Given that all the devices degraded in less than 160 h at virtually the same rate it was concluded that the degradation of the devices within this short time was not due to the long-term effects described above, but rather due to the quick photochemical degradation of P3HT caused by the reaction of the device with O_2 and H_2O from the atmosphere which is accelerated by constant exposure to light.[84–86] The exposure of P3HT to both UV light and oxygen severely damages the polymer structure resulting in the decreased and blue-shifted UV–vis absorption spectra of P3HT.[87] Additionally, the exposure of OSCs to constant illumination has been shown to result in an immediate decay of the V_{oc} of the devices, which is not exhibited by the similar devices not exposed to constant illumination conditions.[88] The results from the lifetime test under constant illumination, however, also show that the stability of the devices with the block copolymers are not any more susceptible to ambient degradation than the reference devices.

**ADVANCED
SCIENCE NEWS**

www.advancedsciencenews.com

**ADVANCED
MATERIALS
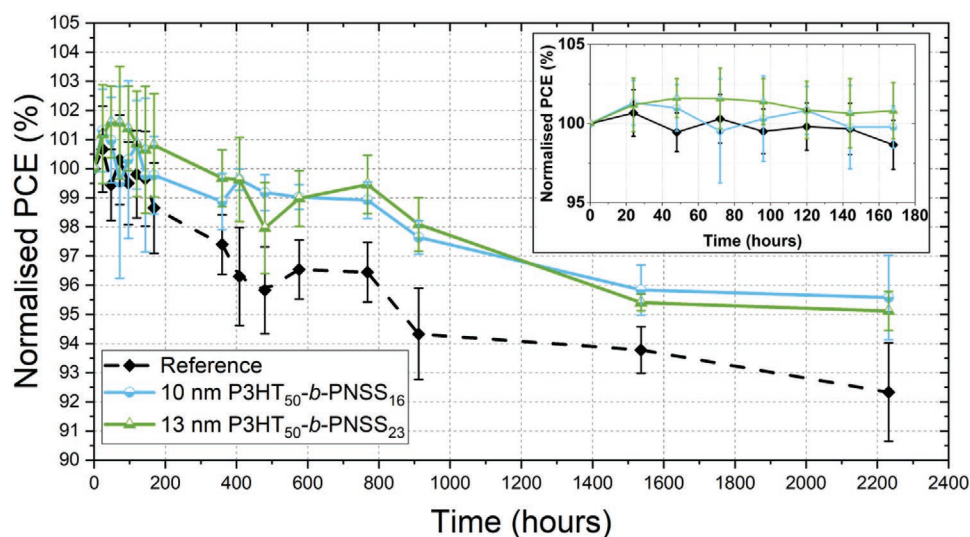INTERFACES**

www.advmatinterfaces.de

Figure 8. Normalized power conversion efficiency as a function of time under constant illumination of a reference device, and devices with 10 nm P3HT$_{50}$-b-PSS$_{16}$ and 13 nm P3HT$_{50}$-b-PSS$_{23}$ films incorporated into them. The shade represents one standard deviation over six measurements for each device.

This is an interesting finding since the devices with a block copolymer have an additional layer that could have provided an additional route towards the degradation of the device.

To determine if the block copolymers prevent long term degradation mechanisms (e.g., chemical reactivity), a second set of lifetime experiments were conducted on a new batch of devices this time, the devices were stored in the dark under constant temperature and humidity, and exposed to light only when measured occasionally during a period of 2232 h. This way, the quick photochemical degradation due to the combination of oxygen, water, and light that occurred during the constant illumination test was minimized. The devices were first measured every 24 h over 168 h to obtain multiple data points within the same time period as that used for the constant illumination measurements. As shown in **Figure 9**, none of the devices degraded significantly, and neither did they exhibited different degradation rates during the first 168 h as evidenced by the widely overlapping error bars. These results confirm that the quick decrease in performance of the devices under constant illumination was due to photochemical degradation, and that such period of time is too short to determine if the block copolymers prevent any long-term device degradation mechanisms. The devices were then stored for 192 additional hours and then measured again (at 360 h after fabrication). This time, the reference device showed slightly more degradation (97.40 ± 1.02% normalized PCE) than the device with the block copolymers (98.87 ± 0.96% and

Figure 9. Normalized power conversion efficiency as a function of time of a reference device, and devices with 10 nm P3HT$_{50}$-b-PSS$_{16}$, and 13 nm P3HT$_{50}$-b-PSS$_{23}$ films incorporated into them. The error bars represent one standard deviation from the average value over eight measurements for each device. Devices were kept stored in the dark except when measured. The sub-figure on the top right corner is a magnification of the first 168 h.

**ADVANCED
SCIENCE NEWS**

www.advancedsciencenews.com

**ADVANCED
MATERIALS
INTERFACES**

www.advmatinterfaces.de

99.67 ± 0.97% normalized PCE for the device with the P3HT$_{50}$-b-PSS$_{16}$, and the 13 nm P3HT$_{50}$-b-PSS$_{23}$ films, respectively). The devices were stored again for 552 additional hours, and within that time, measured five more times in which the reference device showed more degradation than the devices with the block copolymers. After a total of 912 h since fabrication, the reference device was clearly more degraded (94.33 ± 1.57% normalized PCE) than the ones with the 10 nm P3HT$_{50}$-b-PSS$_{16}$, and the 13 nm P3HT$_{50}$-b-PSS$_{23}$ (97.64 ± 0.58% and 98.09 ± 0.92% normalized PCE, respectively). Finally, all the devices were stored again for 1320 additional hours (a total of 2232 h since fabrication) and measured twice within that period of time. These two measurements confirmed that the reference device degrades faster than the devices with the block copolymers. The final normalized PCE of the reference device was 92.33±1.69%, while the final normalized PCE of the devices with the 10 nm P3HT$_{50}$-b-PSS$_{16}$ and the 13 nm P3HT$_{50}$-b-PSS$_{23}$ films were 95.58±1.45%, and 95.12±0.67%, respectively. To corroborate these findings, the experiments were repeated by fabricating another batch of devices and testing them under the same conditions (stored in the dark and exposed to light only when measured) for a similar period of time. The results of the replicated experiment followed the same trend as Figure 9 and thus confirmed that the reference device degrades faster than the devices with the block copolymers (see Figure S9 in the Supporting Information). From the constant illumination lifetime results, it is concluded that the ambient conditions affect all devices equally. Therefore, it is highly likely that the improved long-term stability of the block copolymer incorporated devices can be attributed to the prevention of degradation mechanisms such as delamination and chemical reactivity resulting from the contact between PEDOT:PSS and P3HT:acceptor that occur in the reference device.

3. Conclusions

In summary, three variants of a P3HT-b-PSS block copolymer with different PSS block lengths (9, 16, and 23 units per 50 units of P3HT) were incorporated as an interfacial layer between the PEDOT:PSS HTL and P3HT:PCBM PAL in OSCs. It was found that the thickness of the block copolymer layers depends not only on the concentration of the solution and spin-casting speed, but also on the PSS block length, being thinner for longer block lengths. The maximum efficiencies were achieved when a 10 nm thick film and a 13 nm thick film of P3HT$_{50}$-b-PSS$_{16}$ and P3HT$_{50}$-b-PSS$_{23}$ were used, respectively. The improved efficiency is caused mainly by a 9% increase in the V_{oc}, but also by a slight increase of 2.8% and 6.2% in the FF for the P3HT$_{50}$-b-PSS$_{16}$ and P3HT$_{50}$-b-PSS$_{23}$ devices, respectively. Both the improved V_{oc} and FF compensate for a decrease in J_{sc} caused by the light absorption by the block copolymers which results in less light reaching the P3HT:PCBM active layer. A more favorable HOMO level provided by the block copolymer (compared to the HOMO levels of PEDOT) for holes to travel from the P3HT results in the improved V_{oc} of the devices. Additionally, due to a smoother and homogeneous contact between the block copolymer and the P3HT:PCBM layer, and to the better compatibility between the P3HT block with the donor in the PAL and the PSS block with

the HTL, the FF of the devices incorporating P3HT$_{50}$-b-PSS$_{16}$ and P3HT$_{50}$-b-PSS$_{23}$ is improved when the thickness of the block copolymers is ≥9 nm. The best performing devices with block copolymers also exhibited a higher normalized efficiency after 2200 h of storage compared to the reference devices. This was attributed to the block copolymer acting as a barrier to prevent degradation mechanisms caused by the long-term interactions between PEDOT:PSS and P3HT:PCBM. It was also confirmed that the additional block copolymer layer does not increase the vulnerability of the devices to the combined degradation effects of oxygen, water, and light. These results demonstrate that the two blocks within a block copolymer layer can selectively interact with the two different layers adjacent to the block copolymer. Therefore, it is possible to design block copolymers that can selectively and beneficially interact with specific materials to improve the compatibility between those materials at the interfaces within OSC devices. This has been shown to lead to improved stability and efficiency of OSCs. In this study, the block copolymer was specifically designed to interact with P3HT and PEDOT:PSS respectively due to the simplicity of the P3HT:PCBM based device architecture. However, it is proposed that this approach could equally be applied to other higher efficiency materials systems to produce higher efficiency devices with enhanced stability.

4. Experimental Section

Materials: P3HT (95.7% RR, 65 000 M_w), PCDTBT (34 900 M_w, and 16 200 M_n), PCBM (99.0% purity), PC$_{70}$BM (95% purity), encapsulation epoxy, and PEDOT:PSS in aqueous dispersion (1:2.5 ratio) were all purchased from Ossila Ltd. Chlorobenzene and propan-2-ol were purchased from Fisher Scientific International Inc. and deuterated chlorobenzene (D5) was purchased from Cambridge Isotope Laboratories. The block copolymers were synthesized according to Erothu et al.[6] All chemicals were used without further purification or treatment. Encapsulation glass slides and 20 Ω square^{-1} indium tin oxide (ITO) coated substrates (8 pixel pattern) used for device fabrication were also purchased from Ossila Ltd. Menzel-Gläser microscope glass slides were used as substrates for the block copolymer films that were subject to UV–vis spectroscopy measurements, while 425 µm P/boron doped polished silicon wafers purchased from Si-Mat were used as the substrate for the films that were subject to AFM and ellipsometry measurements.

Device Fabrication: ITO coated substrates were washed in an ultrasonic bath for 10 min first in a boiling 1% Hellmanex III/deionized (DI) water solution and subsequently in propan-2-ol. After each sonication, the substrates were rinsed twice in boiling DI water and once in cold DI water. The substrates were then dried using a nitrogen gas flow and cleaned in an oxygen plasma for 5 min. The PEDOT:PSS dispersion was filtered through a 0.45 µm polyvinyl difluoride filter and then spin cast at 5000 RPM for 40 s. The samples were subsequently annealed at 150 °C for 15 min. The block copolymer solutions (in chlorobenzene) were spin cast at different speeds for 40 s and then transferred to a nitrogen filled glovebox to be thermally annealed on a hot plate at 150 °C for 3 h. Afterwards, the samples were taken out of the glovebox and a 25 mg mL^{-1} P3HT:PCBM (1:0.8 ratio in chlorobenzene) or a 20 mg mL^{-1} PCDTBT:PC$_{70}$BM (1:4 ratio in chlorobenzene) solution was spun cast on top at 2000 RPM for 30 s or 800 RPM for 30 s, respectively. These active layer solutions were filtered through a 0.45 µm polytetrafluoroethylene filter before use. The proto-devices were then placed in a thermal evaporator at <2.0 × 10^{-6} mbar vacuum to deposit a 100 nm Al electrode layer. The devices were then thermally annealed (P3HT based devices at 150 °C for 30 min, and PCDTBT based devices at 80 °C for 15 min) and subsequently encapsulated by using epoxy and

glass coverslips and a 15 min UV light curing step. All processing steps, except for the deprotection of the block copolymers were done in air.

UV–Vis Spectroscopy: UV–vis transmission spectra were obtained using an Ocean optics USB2000+ spectrometer and a DT-MINI-2-GS combined deuterium-halogen light source. The samples were prepared by spin casting the solutions at different speeds for 40 s on glass slides previously cleaned with the same procedure used for the device substrates.

Ellipsometry: The thicknesses of the block copolymer films were obtained with a M-2000 ellipsometer (J.A. Woollam Co.) equipped with a CCD camera and the data were a model fitted to a Cauchy function using the manufacturers CompleteEASE software. The samples were prepared by spin casting the solutions at different speeds for 40 s on silicon wafers previously cleaned with the same procedure used for the device substrates.

Ultraviolet Photoelectron Spectroscopy: To obtain the ultraviolet photoelectron spectra of the films, a Kratos Axis Supra X-ray photoelectron spectrometer with a HeI plasma line of 21.2 eV was used. The area of analysis was 110 µm diameter spot and the spectra were collected from ≈20 to -5 eV binding energy, at 0.025 eV intervals with a 10 eV pass energy for one 300 s sweep.

Atomic Force Microscopy: The surface of the block copolymer films was characterized using a Veeco Dimension 3100 AFM with a Nanoscope IV controller and a TESPA-V2 cantilever (37 N m^{-1} nominal stiffness and 320 kHz nominal resonance frequency) in tapping mode. The samples were prepared in the same way as those used for ellipsometry measurements.

Small Angle Neutron Scattering: The small angle neutron scattering (SANS) data were obtained using the LOQ small-angle diffractometer[89] at the ISIS Pulsed Neutron Source (STFC Rutherford Appleton Laboratory, Didcot, UK). A 10 mm diameter pulsed neutron beam with an incident wavelength (λ) range of 2.2–10 Å was directed through the samples to obtain scattering data within a q range of 0.008–0.254 Å^{-1} where theta is half of the scattering angle. The collected data were corrected for detector response, transmission of the sample, and reference scattering using the Mantid data reduction software[90] to obtain absolute intensity versus momentum transfer 1D scattering plots. The reduced data were fitted using the Poly Gauss Coil model[91] in the SasView software.[92] The solutions for the experiment were prepared by dissolving 5 mg of the block copolymers in 0.5 mL of deuterated chlorobenzene. The solutions were stirred for 2 h at 65 °C and then loaded into cells (Hellma Macro-cuvette 404.000-QX 2 mm thickness 404-2-46, Lab Unlimited) for neutron scattering measurements. The scattering length densities of P3HT, PNSS, chlorobenzene and deuterated chlorobenzene were calculated using the NIST Center for Neutron Research online database.[93] The original data can be obtained free from charge through the digital object identifier https://doi.org/10.5286/ISIS.E.RB1720412.

Lifetime: For the lifetime test under constant illumination an Atlas Suntest CPS+ with a 1500 W xenon bulb, quartz IR reducing filters, and internal reflectors was used.[94] The lamp spectrum approximately matches AM1.5G.[95] The combined bulb and internal reflectors irradiance was 100 mW cm^{-2}. The PCE values reported are normalized to seven silicon photodiodes that take into account fluctuations in the illumination intensity. The applied bias was swept from 0 to 1 V in 0.01 V intervals with a Keithley 2400 source measurement unit. Devices were held at open circuit between measurements with every device being scanned every 15 min and were not masked during the measurements. A total of six measurements per device, per time unit were obtained to calculate the average values shown in Figure 8. Metrics are normalized to their initial values. The temperature of the devices inside the Suntest was 42 ± 3 °C during operation. For the lifetime test not under constant illumination the devices were measured as described in the device performance characterization section immediately after fabrication and then were stored in the dark at 20 °C 30–40% relative humidity until the next measurement. A total of eight measurements per sample were made and averaged to obtain the values shown in Figure 9.

Supporting Information

Supporting Information is available from the Wiley Online Library or from the author.

Conflict of Interest

The authors declare no conflict of interest.

[1] H. Hoppe, N. S. Sariciftci, *J. Mater. Res.* **2004**, *19*, 1924.
[2] K. K. Sadasivuni, K. Deshmukh, T. N. Ahipa, A. Muzaffar, M. B. Ahamed, S. K. K. Pasha, M. A. Al-Maadeed, *J. Mater. Sci. Mater. Electron.* **2019**, *30*, 951.
[3] N. Espinosa, R. García-Valverde, A. Urbina, F. C. Krebs, *Sol. Energy Mater. Sol. Cells* **2011**, *95*, 1293.
[4] R. S. Gurney, D. G. Lidzey, T. Wang, *Rep. Prog. Phys.* **2019**, *82*, 036601.
[5] G. Bernardo, H. Gaspar, G. E. Pérez, A. S. D. Schackleford, A. J. Parnell, M. Bleuel, A. Mendes, S. M. King, S. R. Parnell, *Polym. Test.* **2020**, *82*, 106305.
[6] Y. Liu, J. Zhao, Z. Li, C. Mu, W. Ma, H. Hu, K. Jiang, H. Lin, H. Ade, H. Yan, *Nat. Commun.* **2014**, *5*, 5293.
[7] S. Zhang, L. Ye, W. Zhao, D. Liu, H. Yao, J. Hou, *Macromolecules* **2014**, *47*, 4653.
[8] S. Zhang, Y. Qin, J. Zhu, J. Hou, *Adv. Mater.* **2018**, *30*, 1800868.
[9] C. Yan, S. Barlow, Z. Wang, H. Yan, A. K.-Y. Jen, S. R. Marder, X. Zhan, *Nat. Rev. Mater.* **2018**, *3*, 18003.
[10] Q. Wu, D. Zhao, A. M. Schneider, W. Chen, L. Yu, *J. Am. Chem. Soc.* **2016**, *138*, 7248.
[11] W. Zhao, D. Qian, S. Zhang, S. Li, O. Inganäs, F. Gao, J. Hou, *Adv. Mater.* **2016**, *28*, 4734.
[12] W. Zhao, S. Li, H. Yao, S. Zhang, Y. Zhang, B. Yang, J. Hou, *J. Am. Chem. Soc.* **2017**, *139*, 7148.

[13] B. Fan, D. Zhang, M. Li, W. Zhong, Z. Zeng, L. Ying, F. Huang, Y. Cao, *Sci. China Chem.* **2019**, *62*, 746.

[14] Y. Cui, H. Yao, J. Zhang, T. Zhang, Y. Wang, L. Hong, K. Xian, B. Xu, S. Zhang, J. Peng, Z. Wei, F. Gao, J. Hou, *Nat. Commun.* **2019**, *10*, 2515.

[15] J. Yuan, Y. Zhang, L. Zhou, G. Zhang, H.-L. Yip, T.-K. Lau, X. Lu, C. Zhu, H. Peng, P. A. Johnson, M. Leclerc, Y. Ulanski, Y. Li, Y. Zou, *Joule* **2019**, *3*, 1140.

[16] Q. Liu, Y. Jiang, K. Jin, J. Qin, J. Xu, W. Li, J. Xiong, J. Liu, Z. Xiao, K. Sun, S. Yang, X. Zhang, L. Ding, *Sci. Bull.* **2020**, *65*, 272.

[17] J. Zhang, H. S. Tan, X. Guo, A. Facchetti, H. Yan, *Nat. Energy* **2018**, *3*, 720.

[18] S. B. Dkhil, M. Pfannmöller, S. Bals, T. Koganezawa, N. Yoshimoto, D. Hannani, M. Gaceur, C. Videlot-Ackerman, O. Margeat, J. Ackerman, *Adv. Energy Mater.* **2016**, *6*, 1600290.

[19] N. Li, S. D. Perea, T. Kassar, M. Richter, T. Heumueller, G. J. Matt, Y. Hou, N. S. Güldal, H. Chen, S. Chen, S. Langner, M. Berlinghof, T. Unruh, C. J. Brabec, *Nat. Commun.* **2017**, *8*, 14541.

[20] R. Xue, J. Zhang, Y. Li, Y. Li, *Small* **2018**, *14*, 1801793.

[21] C. Kapnopoulos, E. D. Mekeridis, L. Tzounis, C. Polyzoidis, A. Zachariadis, S. Tsimikli, C. Gravalidis, A. Laskarakis, N. Vouroutzis, S. Logothetidis, *Sol. Energy Mater. Sol. Cells* **2016**, *144*, 724.

[22] M. Finn III, C. J. Martens, A. V. Zaretski, B. Roth, R. R. Søndergaard, f. c. Krebs, D. J. Lipomi, *Sol. Energy Mater. Sol. Cells* **2018**, *174*, 7.

[23] R. R. Søndergaard, M. Hösel, F. C. Krebs, *J. Polym. Sci. B Polym. Phys.* **2013**, *51*, 16.

[24] A. T. Kleinschmidt, S. E. Root, D. J. Lipomi, *J. Mater. Chem. A* **2017**, *5*, 11396.

[25] J. Wu, Y. Xu, Z. Yang, Y. Chen, X. Sui, L. Yang, P. Ye, T. Zhu, X. Wu, X. Liu, H. Cao, A. Peng, H. Huang, *Adv. Energy Mater.* **2019**, *9*, 1803012.

[26] T. Soga, S. Kato, S. Kato, N. Kishi, *J. Mater. Sci. Mater. Electron.* **2019**, *30*, 3332.

[27] S. Molamohammadi, S. A. Nia, Y. S. Jalili, *Sustain. Energy Techn.* **2019**, *34*, 43.

[28] A. A. M. Velazquez, D. Canto-Reyes, J. A. Mendez-Gamboa, M. Acosta, *Mater. Lett.* **2019**, *245*, 65.

[29] C. Kong, B. Song, E. A. Mueller, J. Kim, A. J. McNeil, *Adv. Funct. Mater.* **2019**, *29*, 1900467.

[30] M. Dietrich, J. Heinze, G. Heywang, F. Jonas, *J. Electroanal. Chem.* **1994**, *369*, 87.

[31] M. Hokazono, H. Anno, N. Toshima, *J. Electron. Mater.* **2014**, *43*, 2196.

[32] C.-K. Cho, W.-J. Hwang, K. Eun, S.-H. Choa, S.-I. Na, H.-K. Kim, *Sol. Energy Mater Sol. Cells* **2011**, *95*, 3269.

[33] E. Vitoratos, S. Sakkopoulos, E. Dalas, N. Paliatsas, D. Karageorgopoulos, F. Petraki, S. Kennou, S. A. Choulis, *Org. Electron.* **2009**, *10*, 61.

[34] L. B. Groenedaal, F. Jonas, D. Freitag, H. Pielartzik, J. R. Reynolds, *Adv. Mater.* **2000**, *12*, 481.

[35] S. R. Dupont, E. Voroshazi, P. Heremans, R. H. Dauskardt, *Org. Electron.* **2013**, *14*, 1262.

[36] S. R. Dupont, M. Oliver, F. C. Kreb, R. H. Dauskardt, *Sol. Energy Mater Sol. Cells* **2012**, *97*, 171.

[37] A. M. Higgins, S. J. Martin, P. C. Jukes, J. Geoghegan, R. A. L. Jones, S. Langridge, R. Cubitt, S. Kirchmeyer, A. Wehrum, I. Grizzi, *J. Mater. Chem.* **2003**, *13*, 2814.

[38] K. Z. Xing, M. Fahlman, X. W. Chen, O. Inganäs, W. R. Salaneck, *Synth. Met.* **1997**, *89*, 161.

[39] D. M. Huang, S. A. Mauger, S. Friedrich, S. J. George, D. Dumitriu-LaGrange, S. Yoon, A. J. Moulé, *Adv. Funct. Mater.* **2011**, *21*, 1657.

[40] B. Y. Kadem, M. Al-Hashimi, A. S. Hasan, R. G. Kadhim, Y. Rehaq, A. K. Hassan, *J. Mater. Sci. Mater. Electron.* **2018**, *29*, 19287.

[41] Z. Zhao, W. Zhang, X. Zhao, S. Yang, *Organic Solar Cells Materials, Devices, Interfaces, and Modeling*, CRC Press, Boca Raton, London **2015**.

[42] Z. Zhao, X. Chen, Q. Liu, Q. Wu, J. Zhu, S. Dai, S. Yang, *Org. Electron.* **2015**, *27*, 232.

[43] X. Hou, Q. Li, T. Cheng, L. Yu, F. Wang, J. Lin, S. Dai, Y. Li, Z. Tan, *J. Mater. Chem. A* **2015**, *3*, 18727.

[44] C. K. Kwak, G. E. Pérez, B. G. Freestone, S. A. Al-Isaee, A. Iraqi, D. G. Lidzey, A. D. F. Dunbar, *J. Mater. Chem. C* **2016**, *4*, 10722.

[45] G. E. Pérez, G. Bernardo, H. Gaspar, J. F. K. Cooper, F. Bastianini, A. J. Parnell, A. D. F. Dunbar, *ACS Appl. Mater. Interfaces* **2019**, *11*, 13803.

[46] Y. Shi, F. Li, Y. Chen, *New J. Chem.* **2013**, *37*, 236.

[47] C. Yang, J. K. Lee, A. J. Heeger, F. Wudl, *J. Mater. Chem.* **2009**, *19*, 5416.

[48] M. Raïssi, H. Erothu, E. Ibarboure, H. Cramail, L. Vignau, E. Cloutet, R. C. Hiorns, *J. Mater. Chem. A* **2015**, *3*, 18207.

[49] I. Botiz, S. B. Darling, *Macromolecules* **2009**, *42*, 8211.

[50] B. W. Boudouris, C. D. Frisbie, F. A. Hillmyer, *Macromolecules* **2008**, *41*, 67.

[51] D. de Boer, U. Stalmach, P. F. van Hutten, C. Melzer, V. V. Krasnikov, G. Hadziioannou, *Polymer* **2001**, *42*, 9097.

[52] B. Gholamkhass, S. Holdcroft, *Chem. Mater.* **2010**, *22*, 5371.

[53] M. Raïssi, H. Erothu, E. Ibarboure, H. Bejbouji, H. Cramail, E. Cloutet, L. Vignau, R. C. Hiorns, *J. Mater. Chem. A* **2017**, *5*, 7533.

[54] D. Zhou, X. Cheng, H. Xu, H. Yang, H. Liu, F. Wu, L. Chen, Y. Chen, *J. Mater., Chem. A* **2016**, *4*, 18478.

[55] G. Pirotte, J. Kesters, P. Verstappen, S. Govaerts, J. Manca, L. Lutsen, D. Vanderzande, W. Maes, *ChemSusChem* **2015**, *8*, 3228.

[56] M. W. Matsen, F. S. Bates, *Macromolecules* **1996**, *29*, 1091.

[57] L. Leibler, *Macromolecules* **1980**, *13*, 1602.

[58] P. D. Topham, A. J. Parnell, R. C. Hiorns, *J. Polym. Sci. B* **2011**, *49*, 1131.

[59] V. D. Mitchell, D. J. Jones, *Polym. Chem.* **2018**, *9*, 795.

[60] J. E. Houston, S. Richeter, S. Clément, R. C. Evans, *Polym. Int.* **2017**, *66*, 1333.

[61] H. Erothu, J. Kolomanska, P. Johnston, S. Schumann, D. Deribew, D. T. W. Toolan, A. Gregori, C. Dagron-Lartigau, G. Portale, W. Bras, T. Arnold, A. Distler, R. C. Hiorns, P. Mokarian-Tabari, T. W. Collin, J. R. Howse, P. D. Topham, *Macromolecules* **2015**, *48*, 2107.

[62] O. Werzer, K. Matoy, P. Strohriegl, R. Resel, *Thin Solid Films* **2007**, *515*, 5601.

[63] E. Verploegen, R. Mondal, C. J. Bettinger, S. Sok, M. F. Toney, Z. Bao, *Adv. Funct. Mater.* **2010**, *20*, 3519.

[64] S. Grigorian, S. Joshi, U. Pietsch, *IOP Conf. Ser. Mater. Sci. Eng.* **2010**, *14*, 012007.

[65] Y. A. M. Ismail, T. Soga, T. Jimbo, *Int. J. New. Hor. Phys.* **2015**, *2*, 87.

[66] D. Chirvase, J. Parisi, J. C. Hummelen, V. Dyakonov, *Nanotechnology* **2004**, *15*, 1317.

[67] Y. Kim, S. A. Choulis, J. Nelson, D. D. C. Bradley, S. Cook, J. R. Durrant, *J. Mater. Sci.* **2005**, *40*, 1371.

[68] V. Shrotriya, J. Ouyang, R. J. Tseng, G. Li, Y. Yang, *Chem. Phys. Lett.* **2005**, *411*, 138.

[69] N. K. Elumalai, A. Uddin, *Energy Environ. Sci.* **2016**, *9*, 391.

[70] B. Kitchen, O. Awartani, R. J. Kline, T. McAfee, H. Ade, B. T. O'Connor, *ACS Appl. Mater. Interfaces* **2015**, *7*, 13208.

[71] I. Lange, J. Kniepert, P. Pingel, I. Dumsch, S. Allard, S. Janietz, U. Scherf, D. Neher, *J. Phys. Chem. Lett.* **2013**, *4*, 3865.

[72] A. Ergete, F. K. Sabir, Y. Li, T. Yohannes, *J. Photon. Energy* **2015**, *5*, 057209.

[73] Y. Wang, J. Chen, H. D. Kim, B. Wang, R. Iriguchi, H. Ohkita, *Front. Energy Res.* **2018**, *6*, 113.

[74] A. A. Hussein, A. A. Sultan, M. T. Obeid, A. T. Abdulnabi, M. T. Ali, *Int. J. Sci. Eng. Appl. Sci.* **2015**, *1*, 2395.

ADVANCED
SCIENCE NEWS
www.advancedsciencenews.com

ADVANCED
MATERIALS
INTERFACES
www.advmatinterfaces.de

[75] F. Bastianini, G. E. Pérez, A. R. Hobson, S. E. Rogers, A. J. Parnell, M. Grell, A. F. Gutiérrez, A. D. F. Dunbar, *Sol. Energy Mat. Sol. Cells* **2019**, *202*, 110128.

[76] D. Alemu, H.-Y. Wei, K.-C. Ho, C.-W. Chu, *Energy Environ. Sci.* **2012**, *5*, 9662.

[77] K.-B. Kim, Y.-H. Tak, Y.-S. Han, K.-H. Baik, M.-H. Yoon, M.-H. Lee, *Jpn. J. Appl. Phys* **2003**, *42*, L438.

[78] B. Friedel, P. E. Keivanidis, T. J. K. Brenner, A. Abrusci, C. R. McNeill, R. H. Friend, N. C. Greenham, *Macromolecules* **2009**, *42*, 6741.

[79] C.-C. Chen, S. H. Chang, L.-C. Chen, F.-S. Kao, H.-M. Cheng, S.-C. Yeh, C.-T. Chen, W.-T. Wu, Z.-L. Tseng, C. L. Chuang, C.-G. Wu, *Sol. Energy* **2016**, *134*, 445.

[80] M.-H. Jao, H.-C. Liao, W.-F. Su, *J. Mater. Chem. A* **2016**, *4*, 5784.

[81] Z. Ma, Z. Tang, E. Wang, M. R. Andersson, O. Inganäs, F. Zhang, *J. Phys. Chem. C* **2012**, *116*, 24462.

[82] J. Gasiorowski, R. Menon, K. Hingerl, M. Dachev, N. S. Sariciftci, *Thin Solid Films* **2013**, *536*, 211.

[83] A. J. Moulé, M.-C. Jung, C. W. Rochester, W. Tress, D. LaGrange, I. E. Jacobs, J. Li, S. A. Mauger, M. D. Rail, O. Lin, D. J. Bilsky, Y. Qi, P. Stroeve, L. A. Berben, M. Riede, *J. Mater. Chem. C* **2015**, *3*, 2664.

[84] N. Grossiord, J. M. Kroon, R. Andriessen, P. W. M. Blom, *Org. Electron.* **2012**, *13*, 432.

[85] J. A. Hauch, P. Schilinsky, S. A. Choulis, R. Childers, M. Biele, C. J. Brabec, *Sol. Energy Mater Sol. Cells* **2008**, *92*, 727.

[86] V. I. Madogni, B. Kounouhéwa, A. Akpo, M. Agbomahéna, S. A. Hounkpatin, C. N. Awanou, *Chem. Phys. Lett.* **2015**, *640*, 201.

[87] H. Hintz, H.-J. Egelhaaf, L. Lüer, J. Hauch, H. Peisert, T. Chasse, *Chem. Mater.* **2011**, *23*, 145.

[88] C. H. Peters, I. T. Sachs-Quintana, W. R. Mateker, T. Heumueller, J. Rivnay, R. Noriega, Z. M. Beiley, E. T. Hoke, A. Salleo, M. D. McGehee, *Adv. Mater.* **2012**, *24*, 663.

[89] ISIS Neutron and Muon Source, LOQ specifications, https://www.isis.stfc.ac.uk/Pages/Loq-technical-information.aspx, (accessed: May 2019).

[90] O. Arnold, J. C. Bilheux, J. M. Borreguero, A. Buts, S. I. Campbell, L. Chapon, M. Doucet, N. Draper, R. F. Leal, M. A. Gigg, V. E. Lynch, A. Markvardsen, D. J. Mikkelson, R. L. Mikkelson, R. Miller, K. Palmen, P. Parker, G. Passos, T. G. Perring, P. F. Peterson, S. Ren, M. A. Reuter, A. T. Savici, J. W. Taylor, R. J. Taylor, R. Tolchenov, W. Zhou, J. Zikovsky, *Nucl. Instrum. Methods Phys. Res. A* **2014**, *764*, 156.

[91] SasView, Poly Gaus Coil Model, http://marketplace.sasview.org/models/37/, (accessed: May 2019).

[92] SasView, SasView Software, http://www.sasview.org/, (accessed: May 2019).

[93] National Centre for Nuclear Robotics, Neutron activation and scattering calculator, https://www.ncnr.nist.gov/resources/activation/ (accessed: May, 2019).

[94] M. Wong-Stringer, O. S. Game, J. A. Smith, T. H. Routledge, B. A. Alqurashy, B. G. Freestone, A. J. Parnell, N. Vaenas, V. Kumar, M. O. A. Alawad, A. Iraqi, C. Rodenburg, D. G. Lidzey, *Adv. Energy Mater.* **2018**, *8*, 1801234.

[95] C. Bracher, B. G. Freestone, D. K. Mohamad, J. A. Smith, D. G. Lidzey, *Energy Sci. Eng.* **2018**, *6*, 35.

2000918 (14 of 14)